



Liquid crystalline droplets in aqueous environments: electrostatic effects

Cite this: DOI: 10.1039/c8sm01529e

Alexander V. Dubtsov,^{id}*^a Sergey V. Pasechnik,^{id}^a Dina V. Shmeliova,^{id}^a
 Ayvr Sh. Saidgaziev,^{id}^a Ekaterina Gongadze,^{id}^b Aleš Iglič,^{id}^b and Samo Kralj,^{id}^{cd}

We demonstrate the strong impact of electrostatic properties on radial–bipolar structural transitions in nematic liquid crystal (LC) droplets dispersed in different aqueous environments. In the experimental part of the study, we systematically changed the electrostatic properties of both LC droplets and aqueous solutions. Mixtures of nematics were studied by combining LC materials with negative (azoxybenzene compounds) and strongly positive (cyanobiphenyl) dielectric anisotropy. The aqueous solutions were manipulated by introducing either polyvinyl alcohol, glycerol, electrolyte or amphiphilic anionic surfactant SDS into water. In the supporting theoretical study, we identified the key parameters influencing the dielectric constant and the electric field strength of aqueous solutions. We also estimated the impact of different electrolytes on the Debye length at the LC–aqueous interface. The obtained results are further analysed for chemical and biological sensing applications.

Received 26th July 2018,
 Accepted 2nd November 2018

DOI: 10.1039/c8sm01529e

rsc.li/soft-matter-journal

1 Introduction

Uniaxial nematic liquid crystals (LCs) are anisotropic fluids exhibiting long-range orientational ordering. The mesoscopic local uniaxial orientation of LC molecules is well determined by the nematic director field, displaying head-to-tail invariance.¹ In thermotropic LCs, nematic ordering appears *via* a continuous symmetry breaking phase transition on lowering the temperature from the isotropic phase. Consequently, nematic ordering exhibits softness and is extremely susceptible to various perturbations. For this reason, in flat thin LC cells, in which relatively uniform nematic director configurations are desired, an aligning layer is commonly introduced to suppress perturbations imposed by bare “disordered” substrate structure. In traditional studies, such aligning layers impose either homogeneous or isotropic tangential, tilted or homeotropic anchoring conditions.

These conditions could also be controlled sensitively in curved (*e.g.* spherical or cylindrical) confinements in the absence of alignment layers. Examples are demonstrated in Fig. 1, where nematic director structures^{2,3} in a spherical confinement reveal compromises among elastic properties, determined by the Frank nematic elastic constants K_{11} , K_{22} , K_{33} , and K_{24} , confining

interface conditions and the confinement characteristic size. The most common director configuration for tangential anchoring is the bipolar^{4,5} configuration (Fig. 1A), which is commonly stable in LCs with $K_{11} < K_{33}$. For cases $K_{11} > K_{33}$, twisted bipolar⁶ (Fig. 1B) or toroidal⁷ (Fig. 1C) director configurations are typically observed depending on the K_{22} module value. Homogeneous homeotropic anchoring in the nematic droplets results in a radial-type configuration (Fig. 1G), where the nematic director is preferentially aligned along the radius vector.^{4,5} The tangential-to-homeotropic anchoring transition induces intermediate director configurations (Fig. 1D–F). We, henceforth, use the notations radial and bipolar for the radial-type and bipolar-type nematic structures, respectively.

Confined nematic structures could be efficiently modified by external electric fields,^{8–10} magnetic fields,^{11,12} temperature fields⁴ and flow fields.¹³ Furthermore, a light-induced bipolar-to-radial structural transition can be observed in droplets of photosensitive liquid crystals exhibiting *trans-cis* isomerization,^{14,15} as well as liquid crystals doped with photosensitive azodendrimers.^{16,17} In this case, the wavelength of irradiating light allows controlling forward and reverse transitions.^{16,17} Surface anchoring conditions in spherical LC droplets can be also modified by amphiphilic molecules in confining matrices.^{5,18–21}

Changes in nematic configurations are often accompanied by transformations of topological defects which obey topological conservation laws.^{22,23} Recent results have shown that topological defects can be a platform for the self-organization of biological inclusions.^{24,25} On this basis, LC emulsions with structural transformations within droplets were proposed as a

^a Problem Laboratory of Molecular Acoustics, MIREA – Russian Technological University, 119454, 78 Vernadsky Avenue, Moscow, Russia. E-mail: alexanderdubtsov@gmail.com

^b Faculty of Electrical Engineering, University of Ljubljana, Tržaška 25, 1000 Ljubljana, Slovenia

^c Department of Physics, Faculty of Natural Sciences and Mathematics, University of Maribor, Koroška cesta 160, SI-2000 Maribor, Slovenia

^d Condensed Matter Physics Department, Jožef Stefan Institute, Jamova 39, 1000, Ljubljana, Slovenia

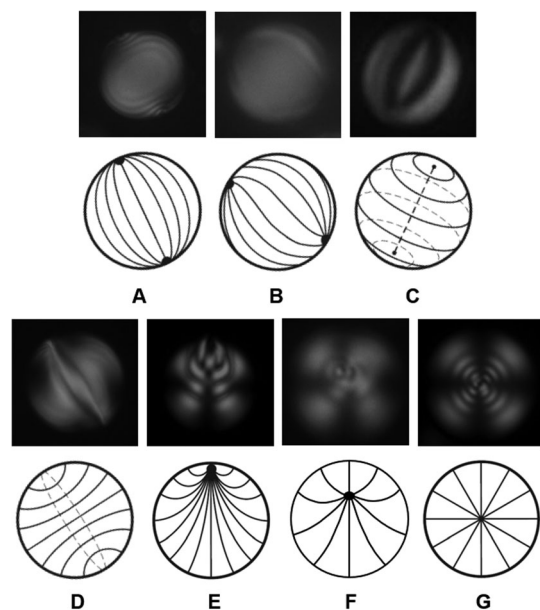


Fig. 1 Typical microscopic grayscale images (upper panels) and corresponding internal ordering (lower panels) of nematic microdroplets for tangential (A–C) and homeotropic (D–G) anchoring conditions: (A) bipolar, (B) twist bipolar, (C) toroidal, (D) axial with line defect, (E) preradial, (F) escaped radial, and (G) radial structures.

sensing platform for chemical and biological impurities.²⁶ Specifically, the sensitivity of LC droplets was found to be six orders of magnitude lower than planar LC interfaces.²⁷ Thereby, structural transformations within droplets are of special interest. These transformations depend on the concentration of biological impurities, the size of LC droplets, the ionic strength and pH of the solution, temperature, and the chemical structure of the LC. Flow cytometry²⁸ and whispering gallery mode (WGM)²⁹ can be used for rapid determination of the internal structure of droplets. In particular, WGM allows one to detect small changes in the internal ordering of LC droplets.²⁹

Recently, spontaneous formation of the radial nematic director configuration was reported in droplets of LC mixtures (consisting of azoxybenzene and biphenyl components) dispersed in water.¹⁵ On the other hand, pure nematic materials in droplets were oriented tangentially at the aqueous–LC interface. A simple theoretical model was presented assuming that electrostatic interactions were the key reason for observed features.¹⁵ However, deeper understanding of electrostatic phenomena is needed to develop future LC–water based sensors for various applications.

In this paper, we report on our experimental and theoretical study of droplets of nematic mixtures that are immersed in aqueous environments consisting of (i) aqueous–PVA, (ii) aqueous–glycerol, (iii) aqueous–electrolyte and (iv) aqueous–SDS solutions.

2 Experimental set-up

We performed the experiments with nematic LCs ZhK-440 (NIOPIK) and 5CB (Alfa Aesar) and their mixtures (Fig. 2).

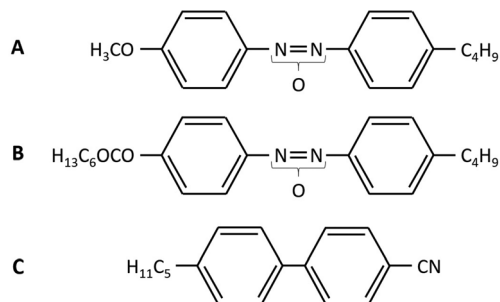


Fig. 2 Chemical formula of the two components LC ZhK-440 (A and B) and the single component LC 5CB (C) used in the experiments.

ZhK-440 is a weakly polar mixture of two-thirds *p*-*n*-butyl-*p*-methoxyazoxybenzene and one-third *p*-*n*-butyl-*p*-heptanoylazoxybenzene with negative dielectric anisotropy ($\Delta\epsilon = -0.4$).^{30,31} A nematic single component 5CB (4-*n*-pentyl-4-cyanobiphenyl) was used as a highly polar liquid crystal with a positive dielectric anisotropy ($\Delta\epsilon = +11.5$). Both pure liquid crystals and their mixtures were studied, where the concentration of 5CB was varied in the range $c = 0 \dots 0.1$ (wt fraction). An aqueous emulsion with micrometer-sized LC droplets (1 to 12 μm) was prepared by sonication and vortex mixing of 2 μl of LC in 2 ml of deionized water (Alfa Aesar). Aqueous solutions of PVA (1%), SDS ($10^{-3} \dots 10^{-6} \text{ g ml}^{-1}$), NaCl and NaOH (all supplied from Labtech, Russia) were used for manipulation of the interfacial anchoring and internal ordering of LC microdroplets. NaCl and NaOH increased the ionic strength and pH of the emulsion to create an electrical double layer at the aqueous–LC interface. The aqueous electrolyte solution was obtained by dissolving both NaCl and NaOH in deionized water to reach salt concentrations of $C_s = 0.1$ and 1 M and $\text{pH} = 11.2$. 4 μl of the LC emulsion was added to 40 μl of the aqueous solution of PVA (or electrolytes, or SDS) which was preliminary dispensed onto cleaned glass substrates by a micropipette (Fisher Scientific) with apyrogenic tips (Sartorius). To study the influence of aqueous glycerol solutions on the internal ordering of LC droplets, glycerol (Panreac Quimica) initially was placed in the glass vials (Fisher Scientific) followed by addition of LC. Polydispersed LC droplets in glycerol were obtained by an aspiration/injection technique using apyrogenic syringes. Step-by-step addition of deionized water to the LC-in-glycerol emulsion allowed us to characterize nematic droplets in the aqueous glycerol solution with a variation of the water concentration from 0% to 95%. Vials with the emulsions were vortexed for 5 minutes to get more uniform water–glycerol mixtures before the optical characterization of LC droplets.

The optical texture of the LC droplets was characterized after a minute of introducing the LC emulsion to the modified aqueous medium. Emulsions with LC droplets were observed using a polarized optical microscope where time dependent images were collected with a digital camera. An objective with 100 \times magnification was used for observation and characterization of micrometer-sized LC droplets. The internal ordering of LC droplets was analyzed by observation of the emulsion in dark (crossed polarizers) and bright (polarized light with switched

off analyzer) fields. The measurements were performed at room temperature $T \sim 26$ °C.

3 Theoretical modeling

Our aim is to analyze the impact of effective electrostatic properties of water solutions on nematic ordering within dispersed LC droplets. For this purpose, we first calculate the relative permittivity ϵ_w of water. Next, we calculate the electric potential and electric field strength of water solutions in contact with a flat negatively charged surface. The derivation gives insight into the influence of an electric double layer at the LC droplet–water interface and ways to manipulate it.

3.1 Relative permittivity of water

The relative permittivity of water is given by $\epsilon_w = 1 + P/(\epsilon_0 E)$, where P is the total polarization of water dipoles, E is the electric field, and ϵ_0 is the permittivity of vacuum. The total polarization $P = P_e + P_0$ consists of the electronic polarization (P_e) and of the polarization contribution of permanent water dipoles (P_0). The electronic polarization determines the refractive index of water $n^2 = 1 + P_e/(\epsilon_0 E) \sim 1.8$ and ϵ_w could be expressed as

$$\epsilon_w = n^2 + \frac{P_0}{\epsilon_0 E}. \quad (1)$$

To obtain the expression for P_0 , we assume that each water molecule possesses an internal dipole of strength p . At a mesoscopic level it holds

$$P_0 = n_w p \langle \cos \theta \rangle, \quad (2)$$

where n_w is the number density of water molecules, θ determines the angle between \vec{p} and the local effective (the so called *cavity*) electric field \vec{E}_c acting on it, and $\langle \dots \rangle$ labels statistical averaging. To estimate $\langle \cos \theta \rangle$, we need an expression for \vec{E}_c . For this purpose, we approximate a water molecule by a sphere with permittivity n^2 possessing an internal point-like water dipole \vec{p} at the center,^{32,33} experiencing field \vec{E}_c , see Fig. 3. The relative permittivity of the surrounding medium, where a spatially homogeneous field \vec{E} is present, is labelled by ϵ_w .

Neglecting the short range interactions between dipoles, the local electric field strength at the centre of the sphere at the location of the permanent (rigid) point-like dipole (Fig. 3) can

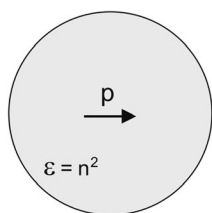


Fig. 3 A single water molecule is modelled by a sphere with relative permittivity n^2 , where $n = 1.33$ is the optical refractive index of water. A permanent point-like rigid dipole with magnitude p is located at the center of the sphere. It experiences the so called cavity field due to the built up charge at the interface between the media.

be expressed as³³ $E_c = \left(\frac{3\epsilon_w}{2\epsilon_w + n^2} \right) E$. Since $\epsilon_w \gg n^2$ (for small enough E) it follows

$$E_c = \frac{3}{2} E. \quad (3)$$

Therefore, the potential energy of \vec{p} in the local field \vec{E}_c can be expressed as^{33,34}

$$W_d = -\vec{p} \cdot \vec{E}_c = \gamma p_0 E \cos(\omega), \quad (4)$$

where $\omega = \pi - \theta$ describes the orientation of the dipole moment vector with respect to $-\vec{E}_c$,

$$\gamma = \frac{(2 + n^2)}{2}, \quad (5)$$

and p_0 is the magnitude of the external dipole of a single isolated water molecule in vacuum.^{33,34} With this in mind we can calculate the statistical average in eqn (2). It follows

$$\langle \cos \omega \rangle = \frac{\int_0^\pi \cos \omega e^{-\gamma p_0 E \beta \cos(\omega)} 2\pi \sin \omega d\omega}{\int_0^\pi e^{-\gamma p_0 E \beta \cos(\omega)} 2\pi \sin \omega d\omega} = -L(\gamma p_0 E \beta). \quad (6)$$

Here $\beta = 1/kT$, k stands for the Boltzmann constant, T is the absolute temperature, and $L(u) = \coth(u) - 1/u$ is the Langevin function. By taking into account eqn (1), (2) and (6) one can express the relative water permittivity ϵ_w as^{32–34}

$$\epsilon_w = n^2 + \frac{n_w p_0}{\epsilon_0} \left(\frac{2 + n^2}{3} \right) \frac{L(\gamma p_0 E \beta)}{E}. \quad (7)$$

In the limit of vanishing electric field strength ($E \rightarrow 0$), the above expression for the relative permittivity of water yields the Onsager limit

$$\epsilon_w = n^2 + \frac{n_w p_0^2 \beta}{2\epsilon_0} \left(\frac{2 + n^2}{3} \right)^2. \quad (8)$$

For $p_0 = 3.1$ D and $n_w/N_A = 55$ mol l^{-1} ,^{32,34} where N_A is the Avogadro number, eqn (8) yields the value $\epsilon_w = 78.5$ at room temperature, which is in good agreement with the experimentally measured value.

3.2 Electric double layer

Next, we consider the change in the electrical properties of water in contact with the charged surface in the presence of the ions of the electrolyte. In the interface between a charged surface and electrolyte solution, there are strong interactions between the charged surface and ions/molecules in the solution, which result in the formation of an electric double layer (EDL).^{35,36} In an EDL the counterions are accumulated close to the charged surface and the coions are depleted from this region. Fig. 4 shows schematics of an EDL near a negatively charged surface and the geometry of our model. We assume that the variational parameters depend only on a single coordinate x .

The finite size of ions in an EDL has been first incorporated by Stern³⁷ with the so-called distance of closest approach (b) (see Fig. 4) and later developed further by Bikerman, Eigen, Wicke and Freise.^{38–41} Their work was upgraded in several later studies.^{42–53}

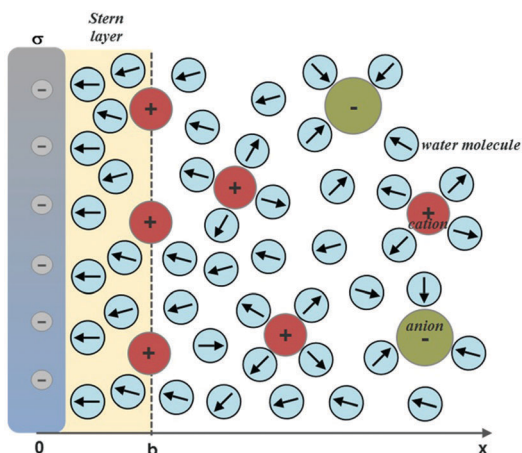


Fig. 4 Schematic figure of an EDL near a negatively charged surface, which mimics the LC–aqueous interface. The water dipoles in the vicinity of the charged surface are partially oriented towards the surface.

Considering the finite and different (asymmetric) size of cations and anions, the expressions for the spatial distribution of the monovalent cations ($n_+(x)$), anions ($n_-(x)$) and water molecules ($n_w(x)$) and the orientational ordering of water dipoles in the electric double layer near a charged surface can be derived using the method of lattice statistics with Boltzmann correction factors.^{32,34} This approach is equivalent to the method based on minimization of the free energy of the system.^{54–57}

In the lattice approach,³⁴ the parameters α_+ and α_- are the number of lattice sites occupied by a hydrated positive and negative ion, respectively³⁴ (see Fig. 5). A single water molecule occupies just one lattice site, therefore $n_s/N_A = 55 \text{ mol l}^{-1}$ is equal to the concentration of pure water, where n_s is the number

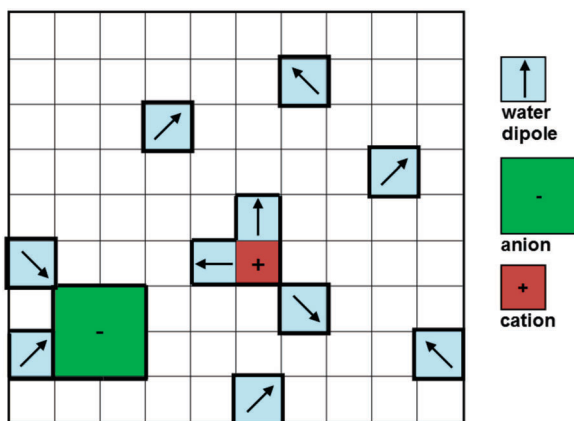


Fig. 5 In the described lattice model of an EDL³⁴ the single positive ion and the single negative ion, each of them together with the surrounding strongly interacting water molecules, which do not contribute to the orientational ordering/polarization in the solution, occupy α_+ and α_- lattice sites, respectively. In the model, the water molecules (and ions) which contribute to α_+ and α_- give rise to electronic polarization only, captured by the term n^2 in the expression for the relative permittivity (eqn (16)). In this schematic figure $\alpha_+ = 4$ and $\alpha_- = 6$. A single free water molecule occupies just one lattice site.

density of lattice sites. In the model a single ion surrounded by strongly interacting water molecules (in the first hydration layer, see Fig. 5) does not contribute to the orientational ordering/polarization in the solution. Namely, orientations of permanent dipoles of water surrounding an ion are frozen-in by the ion's local field. A similar assumption was used in ref. 58. We set that all lattice sites are occupied. The corresponding number densities obey the conservation equation

$$n_s = \alpha_+ n_+(x) + \alpha_- n_-(x) + n_w(x), \quad (9)$$

where $n_+(x)$, $n_-(x)$, and $n_w(x)$ are the number densities of monovalent cations, monovalent anions, and of free water molecules, respectively, and x is the distance from the negatively charged planar surface (see Fig. 4). Quantity α_+ (α_-) determines the number of lattice sites occupied by positive (negative) ions and neighboring strongly interacting water molecules, which do not contribute to the orientational polarization.

The number densities $n_+(x)$ and $n_-(x)$ and the number density of free water molecules $n_w(x)$ can be derived by calculating the corresponding probabilities that a single lattice site in the bulk solution is occupied by one of the three particles (*i.e.* hydrated cations, hydrated anions or free water molecules)³⁴

$$n_+(x) = n_0 e^{-e_0 \phi \beta} \frac{n_s}{D_A(\phi, E)}, \quad (10a)$$

$$n_-(x) = n_0 e^{e_0 \phi \beta} \frac{n_s}{D_A(\phi, E)}, \quad (10b)$$

$$n_w(x) = \frac{n_{0w} n_s}{D_A(\phi, E)} \frac{\sinh(\gamma p_0 E \beta)}{\gamma p_0 E \beta}, \quad (10c)$$

weighted by the corresponding Boltzmann factors, where

$$D_A(\phi, E) = \alpha_+ n_0 e^{-e_0 \phi \beta} + \alpha_- n_0 e^{+e_0 \phi \beta} + \frac{n_{0w}}{\gamma p_0 E \beta} \sinh(\gamma p_0 E \beta). \quad (11)$$

Here n_{0w} is the bulk number density of water molecules, n_0 is the bulk number density of anions and cations, e_0 is the unit charge, and ϕ is the electric potential. In the bulk

$$n_s = \alpha_+ n_0 + \alpha_- n_0 + n_{0w}. \quad (12)$$

The corresponding Poisson's equation reads³⁴

$$\frac{d}{dx} \left[\epsilon_0 \epsilon_w(x) \frac{d\phi}{dx} \right] = -\rho(x). \quad (13)$$

The quantity $\rho(x)$ is the macroscopic volume charge density in the solution, given by

$$\rho(x) = e_0 n_+(x) - e_0 n_-(x) = -2e_0 n_s n_0 \frac{\sinh(e_0 \phi \beta)}{D_A(\phi, E)}, \quad (14)$$

where

$$\epsilon_w(x) = n^2 + n_{0w} n_s \frac{p_0}{\epsilon_0} \left(\frac{2 + n^2}{3} \right) \left(\frac{F(\gamma p_0 E \beta)}{D_A(\phi, E) E} \right). \quad (15)$$

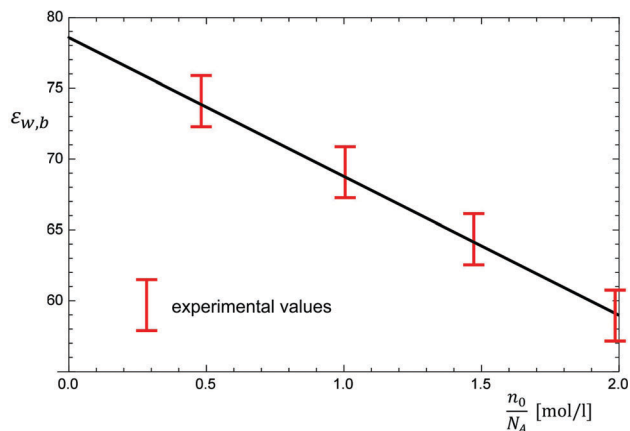


Fig. 6 Calculated dependence of the relative permittivity in bulk electrolyte solution $\varepsilon_{w,b}$ (using eqn (16)) on the bulk salt (NaCl) concentration n_0/N_A . Model parameters are: $(\alpha_+ + \alpha_-) = 7$, optical refractive index $n = 1.33$, $p_0 = 3.1$ D,³⁴ $T = 298$ K and $n_s/N_A = 55$ mol l⁻¹. The experimental values are taken from ref. 59.

Here the function $F(u)$ is defined as $F(u) = L(u)(\sinh u/u)$, where $L(u)$ is the Langevin function. In the limit of vanishing electric field strength ($E \rightarrow 0$) and zero potential ($\phi \rightarrow 0$), we obtain an expression for the bulk relative permittivity

$$\varepsilon_{w,b} = n^2 + \frac{[n_s - (\alpha_+ + \alpha_-)n_0]\beta p_0^2}{2\varepsilon_0} \left(\frac{2+n^2}{3}\right)^2, \quad (16)$$

where we take into account that the number density of water molecules equals $n_{ow} = n_s - (\alpha_+ + \alpha_-)n_0$.

In Fig. 6, we plot the relative permittivity calculated using eqn (16) against increasing salt (NaCl) concentration and compare the results with available experimental measurements.⁵⁹ One sees a relatively good agreement.

Hydration numbers of ions must diminish as their concentration increases.⁶⁰ In an EDL, except in the Stern layer (see Fig. 4), the concentration of counterions is very high, therefore the hydration numbers of counterions in an EDL are diminished relative to the values in the bulk, meaning that in our model $(\alpha_+ + \alpha_-)$ in the EDL close to the charged surface should be smaller than its bulk value. The spatial dependence of $(\alpha_+ + \alpha_-)$ is not included in our model.

The described lattice model of an EDL (eqn (13)–(15)) could include the Helmholtz/Stern layer and the distance of closest approach,⁶¹ which is in general different for cations and anions.^{62–65} We assume that in the Stern layer (Fig. 4) there are no ions, *i.e.*, $n_+(x) = n_-(x) = 0$. Chemisorbed or adsorbed ions are taken into account in the surface charge density σ . Therefore, in the Stern layer the general expression for the relative permittivity (eqn (15)) transforms into

$$\varepsilon_s = n^2 + n_s \frac{p_0}{\varepsilon_0} \left(\frac{2+n^2}{3}\right) \frac{L(\gamma p_0 E \beta)}{E}, \quad (17)$$

where we took $n_w = n_s$. Combining the boundary condition $d\phi/dx(x=0) = -\sigma/\varepsilon_0 \varepsilon_s$ (see Fig. 2) and eqn (17) results in the non-

linear equation for the magnitude of the electric field within the Stern layer^{64,65}

$$\varepsilon_0 E \left(n^2 + n_s \frac{p_0}{\varepsilon_0} \left(\frac{2+n^2}{3}\right) \frac{L(\gamma p_0 E \beta)}{E} \right) = |\sigma|. \quad (18)$$

Inserting the calculated value of E in eqn (17) gives the value of the relative permittivity in the Stern layer (ε_s) for a given surface charge density σ . The relative permittivity in the Stern layer ε_s strongly decreases with the increasing magnitude of σ as the result of saturation of the orientational ordering of water dipoles in the strong electric field of the Stern layer at larger values of σ .^{33,34,64,65}

Note that the system of eqn (17) and (18) can be also used to calculate the relative permittivity (eqn (7)) and the magnitude of electric field strength (E) in the system without NaCl ions (*i.e.* in pure water) in contact with the charged surface having the surface charge density σ , where $n_s/N_A = n_w/N_A = 55$ mol l⁻¹. The corresponding results for the pure water system are presented in Fig. 8 (dashed lines).

The equations of the described lattice model³⁴ taking into account also the Stern layer can be thus written in compact style as

$$\frac{d}{dx} \left[\varepsilon_0 \varepsilon_r(x) \frac{d\phi}{dx} \right] = \begin{cases} 0, & 0 \leq x < b \\ 2e_0 n_s n_0 \frac{\sinh(e_0 \phi \beta)}{D_A(\phi, E)}, & x \geq b, \end{cases} \quad (19)$$

$$\varepsilon_r(x) = \begin{cases} n^2 + n_s \frac{p_0}{\varepsilon_0} \left(\frac{2+n^2}{3}\right) \frac{L(\gamma p_0 E \beta)}{E}, & 0 \leq x < b \\ n^2 + n_{ow} n_s \frac{p_0}{\varepsilon_0} \left(\frac{2+n^2}{3}\right) \left(\frac{F(\gamma p_0 E \beta)}{D_A(\phi, E) E}\right), & x \geq b \end{cases}, \quad (20)$$

where $n_{ow} = n_s - (\alpha_+ + \alpha_-)n_0$.

In the limit of small bulk ion concentrations and small magnitudes of electric potential and assuming $\alpha_+ = \alpha_- = 1$, the described lattice model of the EDL transforms into the modified Langevin Poisson–Boltzmann (LPB) model of the EDL for point-like ions:³²

$$\frac{d}{dx} \left[\varepsilon_0 \varepsilon_r(x) \frac{d\phi}{dx} \right] = \begin{cases} 0, & 0 \leq x < b \\ 2e_0 n_0 \sinh(e_0 \phi \beta), & x \geq b \end{cases} \quad (21)$$

$$\varepsilon_r(x) = n^2 + n_w \frac{p_0}{\varepsilon_0} \left(\frac{2+n^2}{3}\right) \frac{L(\gamma p_0 E \beta)}{E} \quad (22)$$

with $n_w/N_A = 55$ mol l⁻¹. The ion distribution functions are given by $n_+(x) = n_0 e^{-e_0 \phi \beta}$ and $n_-(x) = n_0 e^{+e_0 \phi \beta}$. The finite volumes of ions and water in the electrolyte solution are not taken into account in above $n_+(x)$ and $n_-(x)$ within the LPB model.

The equations of our lattice model (modified GI model)³⁴ were solved numerically for a planar geometry using the FEM method within the COMSOL Multiphysics v. 5.3a software and are plotted in Fig. 7 and 8.

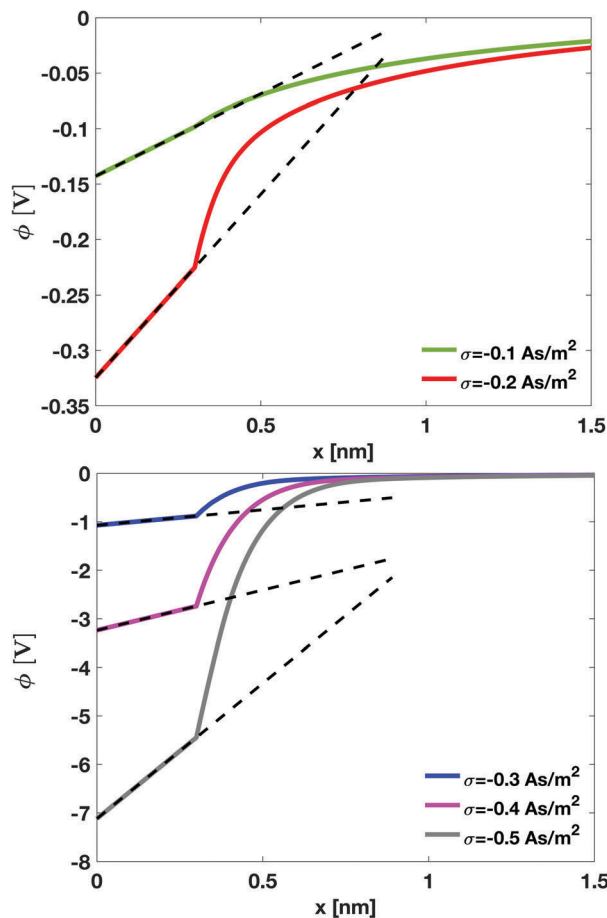


Fig. 7 Electric potential ϕ as a function of the distance from the charged planar surface x within the modified modified GI lattice model for five values of the surface charge density; $\sigma = -0.1, -0.2, -0.3, -0.4$ and -0.5 As m^{-2} . The dipole moment of water $p_0 = 3.1 \text{ D}$,³⁴ bulk concentration of salt $n_0/N_A = 0.1 \text{ mol l}^{-1}$, distance of the closest approach $b = 0.3 \text{ nm}$ and $T = 298 \text{ K}$. In the modified GI model the asymmetric finite size of ions is described by $\alpha_+ = 5$ and $\alpha_- = 2$, where $n_s/N_A = 55 \text{ mol l}^{-1}$. The dashed lines represent the results for zero NaCl concentration.

4 Results and discussion

Our interest is to investigate the impact of electrostatic properties on radial-bipolar structural transitions in nematic LC droplets in an aqueous environment. For this purpose, we vary the electrostatic properties of both the LC droplets and their aqueous surroundings. We vary the effective dielectric properties of LC droplets by mixing weakly polar ZhK-440 and highly polar 5CB nematic LCs. In addition, we modify the electrostatic properties of surrounding media by introducing PVA, glycerol, NaCl, and anionic amphiphilic compound SDS into water.

We first studied the orientational structure of LC mixtures within droplets in the presence of an aqueous PVA solution focusing on the spontaneous formation of radial structures. Representative interference textures are shown in line 1 of Fig. 9. Introduction of an aqueous PVA solution to the emulsion with LC droplets based on pure LC compounds did not result in apparent changes in the nematic ordering. Furthermore, in droplets consisting of LC mixtures the exhibited radial structures

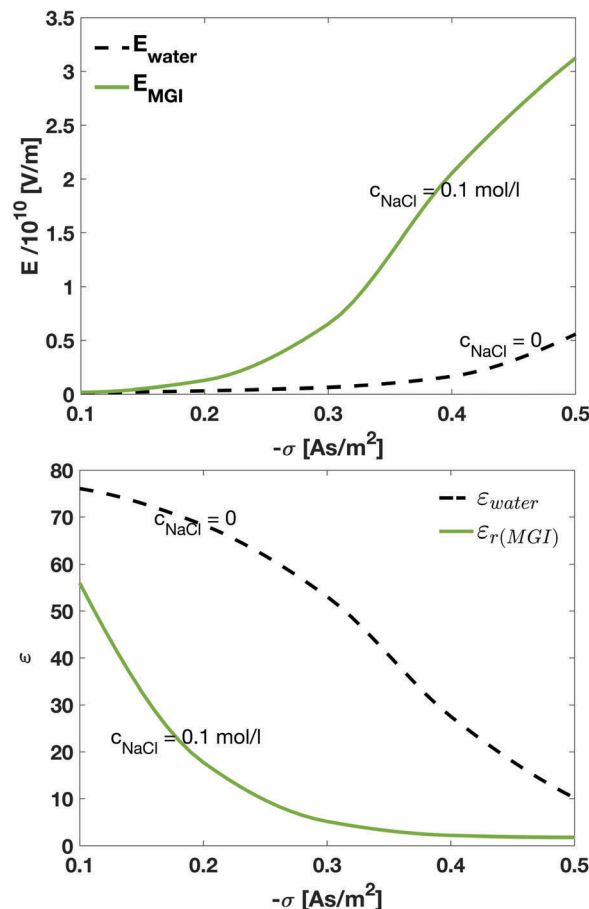


Fig. 8 Calculated magnitude of the electric field strength (upper panel) and the relative permittivity ϵ_s (lower panel) as a function of the magnitude of the surface charge density σ . The calculations were performed for zero NaCl concentration (dashed lines) and NaCl bulk concentration $n_0/N_A = 0.10 \text{ mol l}^{-1}$ (full lines). The values of the model parameters are: $n = 1.33$, $p_0 = 3.1 \text{ D}$, $T = 298 \text{ K}$, and bulk concentration of salt $n_s/N_A = 55 \text{ mol l}^{-1}$.

transformed to the bipolar ones. The analysis of the microscopic textures of the droplets of the emulsion showed an existence of a time dependent bright field in crossed polarizers and two opposite point defects at the poles of the droplet which pointed at tangential anchoring with formation of bipolar configurations. Our observations of the absence of any changes in the internal ordering of droplets with pure LC materials are consistent with previously reported results.^{3,66} Formation of tangential anchoring was observed at interfaces between LCs and solid PVA films, as well at LC-aqueous PVA interfaces. In the latter case, polymer chains tend to be absorbed at the aqueous-LC interface and induce parallel orientation of LC molecules. Moreover, the absorbed weakly polar PVA effectively decreases dipole-dipole interactions at the aqueous-LC interface. Hence, the PVA can be considered as a macroscopic surfactant favouring tangential anchoring. Therefore, if LC droplets with radial structures are formed in an aqueous environment, an increasing concentration of PVA molecules drives the radial-to-bipolar structural transition.

Secondly, we studied internal ordering within droplets consisting of LC mixtures embedded in water-glycerol solutions.

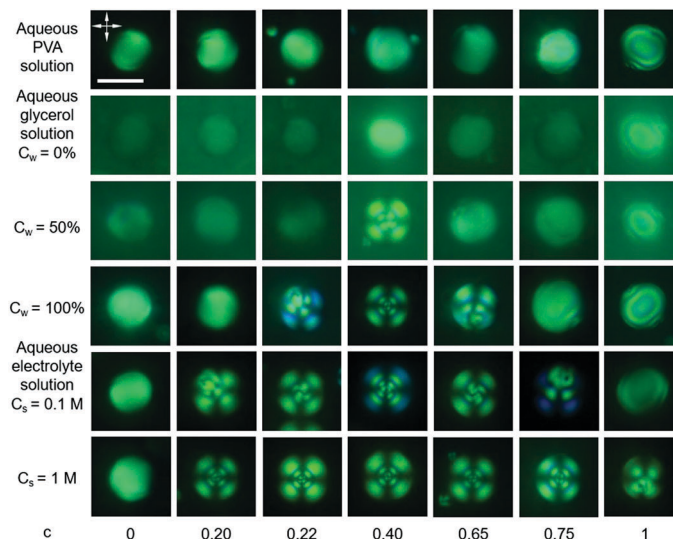


Fig. 9 Microscopic textures of LC droplets at different concentrations $c = 0..1$ of the highly polar component (5CB) in a modified aqueous environment: aqueous PVA (1%) solution; aqueous glycerol solution ($C_w = 0\%..100\%$ is the concentration of water); and aqueous electrolyte solution (pH is increased to 11.2), where $C_s = 0.1, 1 \text{ mol l}^{-1}$ is the NaCl concentration. A green filter was used to protect against negative light irradiation of photosensitive ZhK-440. The double-headed arrows indicate the orientation of polarizers. The scale bar is $10 \mu\text{m}$.

Glycerol commonly provides tangential anchoring for typical LCs.^{4,16,67,68} We established tangential anchoring and formation of bipolar droplets for various LC mixtures in pure glycerol (see row 2 in Fig. 9). No changes in the optical LC textures were observed when the concentration of water in the aqueous glycerol solution increased to $C_w = 30\%$. Further experiments showed that the director configuration within droplets strongly depends on the water concentration in the aqueous glycerol solution. For example, at $C_w = 50\%$ we found the appearance of invariant cross like extinction bands in the crossed polarizers with a point defect in the center of the droplet (revealing the radial configuration) at a concentration of the highly polar component $c = 0.4$ (see row 3

of Fig. 9). Increasing the water concentration to $C_w = 60\%$ ($C_w = 95\%$) resulted in formation of radial droplets at concentrations of $c = 0.35..0.45$ ($c = 0.30..0.55$). In the case of pure deionized water without glycerol ($C_w = 100\%$), radial droplets were observed for concentrations of $c = 0.25..0.60$ (see row 4 in Fig. 9). Therefore, decreasing of the glycerol concentration in glycerol–water solutions broadens the 5CB concentration range where droplets of LC mixtures exhibit radial structures.

Glycerol, like water, is a polar solvent whose molecules have a dipole moment around 2.5 D in solution and around 1.55 D in vapor and a relative permittivity around $\epsilon = 40$.^{69,70} This value of the relative permittivity of glycerol in solution is roughly two times less than that of bulk water ($\epsilon_w = 78.5$) for $p_0 = 3.1 \text{ D}$ and zero electric field strength (see Fig. 10). Therefore, it can be assumed that the effective dipole moment of molecules of the aqueous medium is decreasing if the glycerol concentration is increasing. In Fig. 10, we demonstrate the impact of decreasing single molecule electric dipole moment on the relative permittivity in the aqueous medium calculated by eqn (7), where p_0 is considered as the effective electric dipole per molecule in the glycerol aqueous medium.

For the tested concentrations of 5CB, we estimated the critical concentrations of glycerol below which radial structures are stable for different concentrations of the 5CB LC component. Based on them, we determined the critical effective relative permittivity ϵ_w which is plotted in Fig. 11.

Thirdly, we analyzed the impact of simple electrolytes on the LC ordering. In deionized water, radial structures were stabilized for 5CB concentrations between $c = 0.25$ and $c = 0.60$. When the LC emulsion was added to aqueous 0.1 M NaCl solution at pH 11.2, initial intermediate (preradial) structures at $c = 0.22$ and 0.65 transformed to radial ones (see row 5 of Fig. 9). Thus, radial structures were stabilized in the concentration window

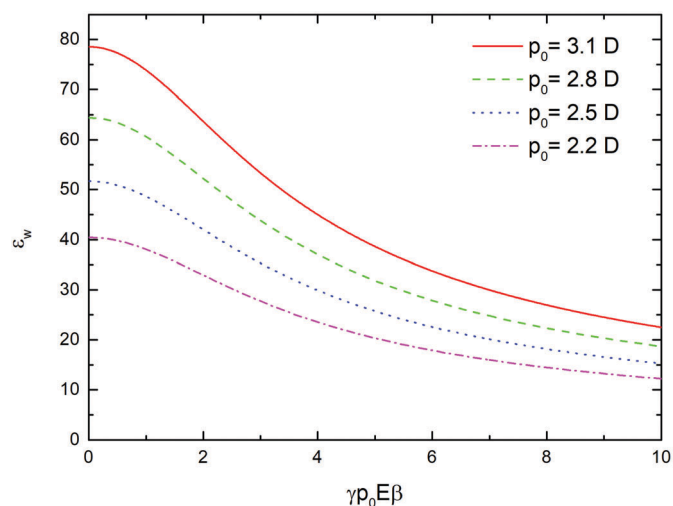


Fig. 10 Dependence of the water relative permittivity on the electric field strength calculated using eqn (7) at room temperature for different values of p_0 : 2.2 D, 2.5 D, 2.8 D and 3.1 D and $n_w/N_A = 55 \text{ mol l}^{-1}$.

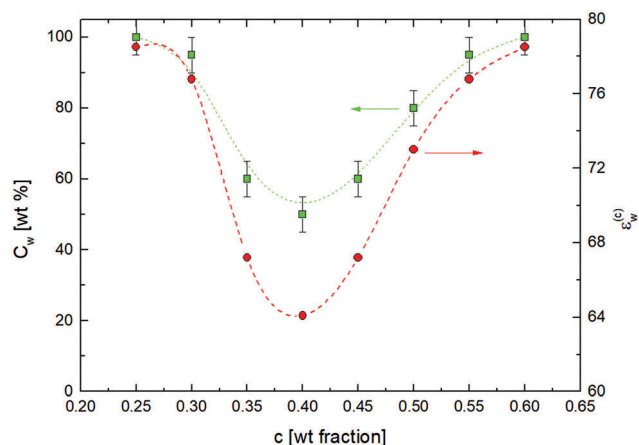


Fig. 11 Dependence of the concentration of water C_w in a water–glycerol solution required for formation of radial droplets on the concentration of the highly polar component in the LC mixture. On the same diagram, we also plotted the critical effective relative permittivity $\epsilon_w^{(c)}$ of the aqueous environment.

$c \in [0.22, 0.65]$. An increase in the salt concentration to 1 M NaCl led to the appearance of radial droplets in the concentration range $c \in [0.20, 0.75]$ (see row 6 of Fig. 9).

Recent studies of planar (non-curved) LC layers confined by water showed that the presence of salts in the water charged the aqueous LC interface. An electric double layer was formed at both sides of the water–LC interface.⁷¹ The appearance of an electric double layer induces a rotational torque tending to reorient dipoles of LC molecules along the electric double layer field lines. An increase in the concentration of salts leads to a decrease in the Debye screening length x_D (see Table 2), which can result in an effective change of boundary conditions. Therefore, further stabilization of the radial droplets of the LC mixtures can be obtained by introducing electrolytes and increasing the local electric field at the aqueous LC interface, *i.e.* at the distance of closest approach $x = b_+$ (see Fig. 8).

In our modelling (see Fig. 7), we calculated the thickness of the double layer by calculating the Debye length x_D (x_D is typically considered as a measure of the thickness of an EDL) as a function of salt concentration (see Table 1). It was determined by the condition $|\phi(x = x_D)| = |\phi(x = 0)|/e$. Table 1 demonstrates that with an increased concentration of ions and

Table 1 The distance x_D where the magnitude of the electric potential drops to the value $|\phi(x = 0)|/e$, calculated within the modified GI lattice model for $b = 0.3$ nm, $p_0 = 3.1$ D, $T = 298$ K, $\alpha_+ = 5$, $\alpha_- = 2$, $n_0/N_A = 55$ mol l⁻¹ and for two values of the surface charge density and different salt concentrations n_0/N_A

n_0/N_A [mol l ⁻¹]	x_D [nm]	
	$\sigma = -0.1$ As m ⁻²	$\sigma = -0.2$ As m ⁻²
0.5	0.45	0.39
0.2	0.58	0.41
0.1	0.71	0.45
0.05	0.88	0.48
0.02	1.15	0.55
0.01	1.45	0.62

with increased surface charge at the interface the double layer shrinks. For example, for $\sigma = -0.1$ As m⁻² we obtain $x_D(n_0 = 0.1)/x_D(n_0 = 0.01) \sim 0.5$, and $x_D(\sigma = -0.2)/x_D(\sigma = -0.1) \sim 0.6$ for $n_0 = 0.1$ mol l⁻¹.

Our experimental data are summarized in Table 2. We can infer that by adding electrolytes into aqueous solutions, the concentration c stability window of radial structures increases through a set of intermediate configurations. For LC mixtures at $c = 0$ and $c = 1$, tangential anchoring within droplets was observed for all dispersed media compositions (aqueous PVA solution, pure water and glycerol, water and glycerol mixtures, and 0.1 M aqueous NaCl solution) except for a stronger electrolyte (1 M NaCl). In the latter case, bipolar droplets occurred at $c = 0$ whereas preradial ones at $c = 1$. A relatively strong electric field, created by the EDL at the electrolyte–LC interface, orients the LC director along/orthogonal to the field lines depending on the sign of the dielectric anisotropy $\Delta\epsilon$ which is determined by the position of a dipole in the nematic molecules. Taking into account dielectric parameters of a weakly polar ZhK-440 ($\Delta\epsilon = -0.4$)³⁰ and a highly polar 5CB ($\Delta\epsilon = +11.5$),⁷² one can conclude that the electric field tends to align the ZhK-440 parallel (5CB perpendicularly) to the aqueous–LC interface consistent with an observation of tangential ($c = 0$) and homeotropic ($c = 1$) anchoring respectively within the droplets (see the lower horizontal line in Table 2 at $C_s = 1$ M). However, a relatively weak electric field (Table 2 at $C_s = 0.1$ M), contrary to $c = 1$ with higher $\Delta\epsilon$, induces homeotropic anchoring in the range $0.2 < c < 0.75$ (bipolar–radial transition in the range $0.22 < c < 0.65$) where $\Delta\epsilon$ of the LC mixtures is lower than for $c = 1$. Such behavior can be explained by variations of both molecular configurations and dielectric properties of LC mixtures.

It is well known that mixtures of weakly and highly polar rod-like mesogens may induce LC complex formation, whose properties strongly depend on the chemical formula of single components.^{73,74} An X ray study of such mixtures revealed that a weakly polar single component of ZhK-440 (depicted in Fig. 2A) is characterized by a monomer density wave corresponding to a fluctuation layer structure, whereas for 5CB both monomer and dimeric density waves take place, which confirms the existence of dimers with an antiparallel direction of dipoles in a nematic phase.⁷⁵ The absence of the dimeric density wave in the mixture (only the monomer density wave was observed) at $0 < c < 0.8$ indicated destroying the 5CB dimers and arising 5CB monomers/LC complexes. It was also reported that the maximal number of LC complexes occurred at a concentration 1 : 1. Further increasing of c in the range $0.8 < c < 1$ showed slight decreasing (appearance/increasing) of the monomer (dimeric) density wave.

Recent an X ray study of Langmuir–Blodgett LC films at electrolyte–LC interfaces revealed a collective effect, where a CN group (providing a strong dipole moment 4 D) of the 5CB monomers (LC complexes) effectively interacts with an aqueous layer depending on the compression.⁷⁶ Therefore, we proposed that increasing c in the range $0 < c < 0.2$ did not induce changes in the tangentially oriented LC mixture because 5CB monomers (LC complexes) are not enough at the interface to

Table 2 Director configurations within droplets of LC mixtures ($c = 0 \dots 1$) confined to a modified aqueous environment, where APS is the aqueous PVA (1%) solution; AGS is the aqueous glycerol solution, where $C_w = 0\% \dots 100\%$ is the concentration of water; AES – the aqueous electrolyte solution ($\text{pH} = 11.2$), where $C_s = 0.1, 1 \text{ mol l}^{-1}$ is the NaCl concentration; and B is the bipolar, R is the radial and I is the intermediate configuration respectively

Environment/ c	0.0	0.10	0.15	0.20	0.22	0.25	0.30	0.35	0.40	0.45	0.55	0.60	0.65	0.75	0.85	1
APS	B	B	B	B	B	B	B	B	B	B	B	B	B	B	B	B
AGS (C_w , %)	0	B	B	B	B	B	B	B	B	B	B	B	B	B	B	B
	40	B	B	B	B	B	B	B	I	B	B	B	B	B	B	B
	50	B	B	B	B	B	B	B	I	R	I	B	B	B	B	B
	60	B	B	B	B	B	B	I	R	R	I	B	B	B	B	B
	95	B	B	B	B	B	I	R	R	R	R	I	B	B	B	B
	100	B	B	B	B	I	R	R	R	R	R	R	I	B	B	B
AES (C_s , M)	0.1	B	B	B	I	R	R	R	R	R	R	R	R	I	B	B
	1	B	I	I	R	R	R	R	R	R	R	R	R	R	I	I

induce bipolar–radial transformation. Meanwhile, in the range $0 < c < 0.2$, we registered decreasing of the SDS concentration (see below), which is needed to induce the bipolar–radial structural transition. Then, at $0.25 < c < 0.6$ the 5CB monomers (LC complexes), adsorbed at the aqueous–LC interface, induce the bipolar–radial transition through a set of configurations observed in the range $0.2 < c < 0.25$. Further increasing c in the range $0.75 < c < 1$ results in the radial–bipolar transition through the gap $0.6 < c < 0.75$ with intermediate structures due to the appearance and increasing of dimeric 5CB molecules. Thus, this behavior allows us to explain the spontaneous bipolar–radial transition shown at $C_w = 100\%$ and $C_s = 0.1 \text{ mol l}^{-1}$ (see Table 2). Meanwhile, the spontaneous bipolar–radial transition arose also in the aqueous glycerol mixture at $C_w = 50\%$. In this case, the non-monotonous (V-shaped) dependence shown in Fig. 11 can be explained by the effects taking place at both sides of the interface (LC adsorbed layer *versus* aqueous/glycerol environment) which mutually reinforce each other. Taking into account the mentioned above maximal concentration of 5CB monomers (LC complexes), which are characterized by the dipole moment $p = 4 \text{ D}$, collective ordering of 5CB monomers (LC complexes) at the aqueous boundary changes the surface charge density at the interface from the LC side. This surface polarization of 5CB monomers (LC complexes) from the LC side involves ordering of water/glycerol dipoles and the following bipolar–radial transition takes place when the effective dipole moment $p = 2.3 \text{ D}$ ($\epsilon_w \sim 60$). Decreasing of the water concentration in the aqueous glycerol solution ($p = 1.55 \text{ D}$ dipole moment of glycerol in a vapor) results in decreasing of water clusters⁷⁷ which suppresses both collective ordering of the 5CB monomers (LC complexes) and the bipolar–radial transition, respectively. At the same time, decreasing of 5CB monomers/LC complexes at $c > 0.4$ and $c < 0.4$ (with a corresponding decrease of effective dipole ordering of 5CB monomers/LC complexes at the LC side) requires stronger dipole ordering of confining environments and the bipolar–radial transition takes place when increasing the water effective dipole from 2.3 D to 3.1 D (ϵ_w from ~ 60 to ~ 80). Quite different behavior of 5CB monolayers at water and glycerol surfaces was also shown by wetting studies.⁷⁸

Finally, we experimentally studied the internal behaviour of LC droplets based on pure materials and their mixtures

confined by water in the presence of an anionic surfactant SDS, which is a synthetic amphiphilic compound. Note that both the ionic and amphiphilic characters favour radial structures. Namely, past studies of the orientational ordering of LCs with flat⁷⁹ and curved⁸⁰ aqueous interfaces containing amphiphilic molecules report transitions from tangential anchoring to homeotropic at some critical concentration of amphiphilic molecules. Because amphiphilic molecules are surfactants with polar heads and hydrophobic tails, they tend to assemble at the water–LC interface, where their hydrophobic tails distort the initial tangential orientation.

We investigated LC droplets with diameter of 4–6 μm in an aqueous SDS solution (SDS concentration of $C_{\text{SDS}} = 10^{-3} \dots 10^{-6} \text{ g ml}^{-1}$) at different concentrations of the highly polar component ($c = 0 \dots 0.2$). Fig. 12A shows panels of microscopic images of LC droplets in water with different concentration of SDS. One sees that the presence of SDS in water strongly favours radial structures. We observe that the critical concentration C_{SDS} stabilizing radial structures linearly decreases with the highly polar component c . For $c = 0.2$, the critical SDS concentration is required to be of an order of magnitude lower than for $c = 0$ (Fig. 12B). Such a dependence indicates that the bipolar–radial transition is induced by the joint action of SDS and 5CB monomers/LC complexes at the aqueous–LC interface, where SDS (5CB monomers) localizes on the aqueous (LC) side. In this case the bipolar–radial transformation at lower C_{SDS} requires higher c or *vice versa*.

5 Conclusions

In summary, we investigated the internal ordering within LC droplets in several aqueous environments. We consider LCs consisting of (i) weakly polar and (ii) strongly polar character, and their (iii) mixtures. The aqueous environments were modified by adding either (i) glycerol, (ii) PVA, (iii) electrolyte, or (iv) amphiphilic anionic SDS into the water solutions. Radial–bipolar structural transitions were observed using optical microscopy.

In the experimental part of the work, we systematically varied electrostatic properties within LC droplets by changing the concentration c of the strongly polar 5CB component in the interval $c \in [0, 1]$. We found that effective tangential anchoring

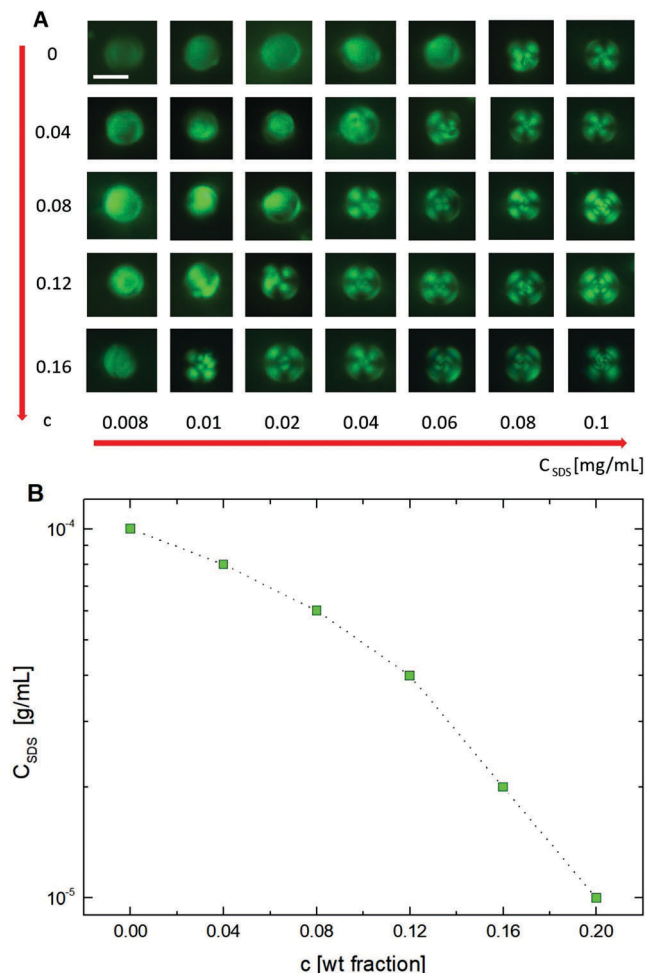


Fig. 12 Microscopic images (A) of the LC droplets with variation of both the highly polar component c in the LC mixture and the concentration of SDS in water. Dependence of the critical SDS concentration which triggers bipolar–radial structural transformation on c (B). Note that LC droplets in water free of SDS at $c = 0.20$ exhibited an axial configuration with a line defect. The scale bar is 5 μm .

was formed in droplets of LC mixtures confined by an aqueous PVA solution, as well as glycerol, while radial configurations could be formed in water–glycerol and water–electrolyte solutions. We found that the formation of radial configurations within droplets of mixtures is strongly dependent on the effective value of the relative permittivity of the dispersed medium. An increase in the relative permittivity in water leads to an increase in the range of concentrations of the strongly polar compound in the LC mixture, where radial structures are stable. Further expansion of the concentration range occurred in the presence of electrolytes. We also triggered the LC structural transitions by introducing anionic surfactant SDS into the water. We found that the concentration of SDS in the water necessary for the structural transformation decreases linearly with the concentration of the highly polar component in the LC mixture. For example, an increase of the highly polar component from 0% to 20% required an order of magnitude lower SDS concentration in water (10^{-5} g ml^{-1} versus 10^{-4} g ml^{-1}).

In the theoretical part, we calculated the relative permittivity ϵ_w of the aqueous environment and determined key parameters affecting its value. We showed that in the bulk ϵ_w linearly decreases on increasing the concentration of hydrated positive and negative ions. We calculated the Debye length (thickness of the EDL) at a negatively charged surface, which in our modelling mimics the LC–aqueous interface, as a function of the surface charge density and concentration of ions. We calculated the shrinking of the Debye length with increasing concentration of ions and/or increasing the surface charge density. We also calculated the electric field strength and the relative permittivity at the charged surface at the distance of closest approach (*i.e.* at $x = b_+$, see Fig. 4) for pure deionized water without the electrolyte and for electrolyte (NaCl) solution (see Fig. 8) in order to explain the observed experimental results showing the dependence of c required for the bipolar–radial transition on the concentration of salts in the medium.

These results are also consistent with our preliminar modelling presented in ref. 15 where the spontaneous formation of radial droplets is caused by electrostatic forces at the water–LC interface. The obtained results showed that mixtures with an appropriate ratio of the components could tune the sensitivity of LC responsive materials to chemical and biological impurities. Moreover pure weakly/highly polar LCs and their mixtures provide different sensing templates for bipolar–radial or radial–bipolar structural transitions within the droplets, respectively.

Conflicts of interest

There are no conflicts to declare.

Acknowledgements

A. V. D. acknowledges the financial support from Ministry of Education and Science of the Russian Federation (grant of the President of Russia for young scientists No. MK-4886.2016.2). S. K., E. G. and A. I. acknowledges the financial support from the Slovenian Research Agency (research core funding No. P1-0099 and No. P2-0232). A. V. D. would like to thank Prof. Oleg Lavrentovich for initiation of the present experimental investigation.

Notes and references

- 1 L. M. Blinov, *Structure and Properties of Liquid Crystals*, Springer, New York, 2011.
- 2 G. P. Crawford and S. Žumer, *Liquid crystals in complex geometries: formed by polymer and porous networks*, CRC Press, London, 1996.
- 3 P. Držaic, *Liquid Crystal Dispersions*, World Scientific, Singapore, 1995.
- 4 G. Volovik and O. Lavrentovich, *Zh. Eksp. Teor. Fiz.*, 1983, **85**, 1997–2010.
- 5 O. O. Prischepa, A. V. Shabanov and V. Y. Zyryanov, *Mol. Cryst. Liq. Cryst.*, 2005, **438**, 141/[1705]–150/[1714].

- 6 P. Drzaic, *Liq. Cryst.*, 1999, **26**, 623–627.
- 7 J. Jiang and D.-K. Yang, *Liq. Cryst.*, 2018, **45**, 102–111.
- 8 V. G. Bondar, O. D. Lavrentovich and V. M. Pergamenschchik, *Zh. Eksp. Teor. Fiz.*, 1992, **101**, 111–125.
- 9 F. Xu, H. Kitzerow and P. Crooker, *Phys. Rev. A: At., Mol., Opt. Phys.*, 1992, **46**, 6535–6540.
- 10 V. Y. Zyryanov, M. N. Krakhalev, O. O. Prishchepa and A. V. Shabanov, *JETP Lett.*, 2007, **86**, 383–388.
- 11 S. Candau, P. L. Roy and F. Debeauvais, *Mol. Cryst. Liq. Cryst.*, 1973, **23**, 283–297.
- 12 A. V. Koval'chuk, M. V. Kurik, O. D. Lavrentovich and V. V. Sergan, *Zh. Eksp. Teor. Fiz.*, 1988, **94**, 350–364.
- 13 A. Fernández-Nieves, D. R. Link, M. Márquez and D. A. Weitz, *Phys. Rev. Lett.*, 2007, **98**, 087801.
- 14 A. V. Dubtsov, S. V. Pasechnik, D. V. Shmeliova and S. Kralj, *Appl. Phys. Lett.*, 2014, **105**, 151606.
- 15 A. V. Dubtsov, S. V. Pasechnik, D. V. Shmeliova, D. A. Semerenko, A. Igljč and S. Kralj, *Liq. Cryst.*, 2018, **45**, 388–400.
- 16 G. Lee, F. Araoka, K. Ishikawa, Y. Momoi, O. Haba, K. Yonetake and H. Takezoe, *Part. Part. Syst. Charact.*, 2013, **30**, 847–852.
- 17 S. A. Shvetsov, A. V. Emelyanenko, N. I. Boiko, J.-H. Liu and A. R. Khokhlov, *J. Chem. Phys.*, 2017, **146**, 211104.
- 18 J. K. Gupta, J. S. Zimmerman, J. J. de Pablo, F. Caruso and N. L. Abbott, *Langmuir*, 2009, **25**, 9016–9024.
- 19 J. K. Gupta, S. Sivakumar, F. Caruso and N. L. Abbott, *Angew. Chem., Int. Ed.*, 2009, **48**, 1652–1655.
- 20 M. C. D. Carter, D. S. Miller, J. Jennings, X. Wang, M. K. Mahanthappa, N. L. Abbott and D. M. Lynn, *Langmuir*, 2015, **31**, 12850–12855.
- 21 A. V. Dubtsov, S. V. Pasechnik, D. V. Shmeliova, S. Kralj and R. Repnik, *Adv. Condens. Matter Phys.*, 2015, 803480.
- 22 M. Kleman and O. D. Lavrentovich, *Soft Matter Physics: An Introduction (Partially Ordered Systems)*, Springer, New York, 2003.
- 23 O. D. Lavrentovich, *Liq. Cryst.*, 1998, **24**, 117–126.
- 24 X. Wang, D. S. Miller, E. Bukusoglu, J. J. de Pablo and N. L. Abbott, *Nat. Mater.*, 2016, **15**, 106–112.
- 25 X. Wang, Y.-K. Kim, E. Bukusoglu, B. Zhang, D. S. Miller and N. L. Abbott, *Phys. Rev. Lett.*, 2016, **116**, 147801.
- 26 R. J. Carlton, J. T. Hunter, D. S. Miller, R. Abbasi, P. C. Mushenheim, L. N. Tan and N. L. Abbott, *Liq. Cryst. Rev.*, 2013, **1**, 29–51.
- 27 I.-H. Lin, D. S. Miller, P. J. Bertics, C. J. Murphy, J. J. de Pablo and N. L. Abbott, *Science*, 2011, **332**, 1297–1300.
- 28 D. S. Miller, X. Wang, J. Buchen, O. D. Lavrentovich and N. L. Abbott, *Anal. Chem.*, 2013, **85**, 10296–10303.
- 29 M. Humar and I. Mušević, *Opt. Express*, 2011, **19**, 19836–19844.
- 30 M. Barnik, S. Belyaev, M. Grebenkin, V. Rummyantsev, V. Seliverstov, V. Tsvetkov and N. Shtykov, *Sov. Phys. Crystallogr.*, 1978, **23**, 451–454.
- 31 D. Aronzon, E. P. Levy, P. J. Collings, A. Chanishvili, G. Chilaya and G. Petriashvili, *Liq. Cryst.*, 2007, **34**, 707–718.
- 32 E. Gongadze, A. Velikonja, S. Perutkova, P. Kramar, A. Maček-Lebar, V. Kralj-Igljč and A. Igljč, *Electrochim. Acta*, 2014, **126**, 42–60.
- 33 E. Gongadze and A. Igljč, *Bioelectrochemistry*, 2012, **87**, 199–203.
- 34 E. Gongadze and A. Igljč, *Electrochim. Acta*, 2015, **178**, 541–545.
- 35 M. Gouy, *J. Phys. Theor. Appl.*, 1910, **9**, 457–468.
- 36 D. L. Chapman, *Philos. Mag.*, 1913, **25**, 475–481.
- 37 O. Stern, *Z. Elektrochem. Angew. Phys. Chem.*, 1924, **30**, 508–516.
- 38 J. J. Bikerman, *Philos. Mag.*, 1942, **33**, 384–397.
- 39 E. Wicke and M. Eigen, *Z. Elektrochem.*, 1952, **56**, 551–561.
- 40 M. Eigen and E. Wicke, *J. Phys. Chem.*, 1954, **58**, 702–714.
- 41 V. Freise, *Z. Elektrochem.*, 1952, **56**, 822–827.
- 42 S. McLaughlin, *Annu. Rev. Biophys. Biophys. Chem.*, 1989, **18**, 113–136.
- 43 C. Outhwaite, *Mol. Phys.*, 1976, **31**, 1345–1357.
- 44 C. Outhwaite, *Mol. Phys.*, 1983, **48**, 599–614.
- 45 S. W. Kenkel and J. R. Macdonald, *J. Chem. Phys.*, 1984, **81**, 3215–3221.
- 46 G. M. Torrie and J. P. Valleau, *J. Chem. Phys.*, 1980, **73**, 5807–5816.
- 47 L. Mier-y-Teran, S. H. Suh, H. S. White and H. T. Davis, *J. Chem. Phys.*, 1990, **92**, 5087–5098.
- 48 V. Kralj-Igljč and A. Igljč, *J. Phys. II*, 1996, **6**, 477–491.
- 49 K. Bohinc, V. Kralj-Igljč and A. Igljč, *Electrochim. Acta*, 2001, **46**, 3033–3040.
- 50 L. B. Bhuiyan and C. W. Outhwaite, *J. Colloid Interface Sci.*, 2009, **331**, 543–547.
- 51 P. Strating and F. Wiegels, *J. Phys. A: Math. Gen.*, 1993, **26**, 3383–3391.
- 52 J. W. Lee, R. H. Nilson, J. A. Templeton, S. K. Griffiths, A. Kung and B. M. Wong, *J. Chem. Theory Comput.*, 2012, **8**, 2012–2022.
- 53 C. Lian, K. Liu, K. L. Van Aken, Y. Gogotsi, D. J. Wesolowski, H. L. Liu, D. E. Jiang and J. Z. Wu, *ACS Energy Lett.*, 2016, **1**, 21–26.
- 54 A. Igljč, D. Drobne and V. Kralj-Igljč, *Nanostructures in Biological Systems: Theory and Applications*, CRC Press, Boca Raton, 2015.
- 55 E. Gongadze, U. van Rienen, V. Kralj-Igljč and A. Igljč, *Comp. Meth. Biomech. Biomed. Eng.*, 2013, **16**, 463–480.
- 56 A. Igljč, E. Gongadze and K. Bohinc, *Bioelectrochemistry*, 2010, **79**, 223–227.
- 57 M. Drab, E. Gongadze, L. Mesarec, S. Kralj, V. Kralj-Igljč and A. Igljč, *Elektrotehniški Vestnik*, 2017, **84**, 221–234.
- 58 K. Giese, U. Kaatz and R. Pottel, *J. Phys. Chem.*, 1970, **74**, 3718–3725.
- 59 J. B. Hasted, D. M. Ritson and C. H. Collie, *J. Chem. Phys.*, 1948, **16**, 1–21.
- 60 Y. Marcus, *J. Phys. Chem. B*, 2014, **118**, 10471–10476.
- 61 M. Lorenzetti, E. Gongadze, M. Kulkarni, I. Junkar and A. Igljč, *Nanoscale Res. Lett.*, 2016, **11**, 378.
- 62 C. W. Outhwaite and L. B. Bhuiyan, *J. Chem. Phys.*, 1986, **84**, 3461–3471.
- 63 J. Yu, G. E. Aguilar-Pineda, A. Antillón, S.-H. Dong and M. Lozada-Cassou, *J. Colloid Interface Sci.*, 2006, **295**, 124–134.
- 64 A. Velikonja, E. Gongadze, V. Kralj-Igljč and A. Igljč, *Int. J. Electrochem. Sci.*, 2014, **9**, 5885–5894.
- 65 A. Velikonja, V. Kralj-Igljč and A. Igljč, *Int. J. Electrochem. Sci.*, 2015, **10**, 1–7.

- 66 G. Petriashvili, M. P. De Santo, R. J. Hernandez, R. Barberi and G. Cipparrone, *Soft Matter*, 2017, **13**, 6227–6233.
- 67 V. G. Nazarenko, A. B. Nych and B. I. Lev, *Phys. Rev. Lett.*, 2001, **87**, 075504.
- 68 X. Wang, Y. Zhou, Y.-K. Kim, D. S. Miller, R. Zhang, J. A. Martinez-Gonzalez, E. Bukusoglu, B. Zhang, T. M. Brown, J. J. de Pablo and N. L. Abbott, *Soft Matter*, 2017, **13**, 5714–5723.
- 69 H. A. Rizk and I. M. Elanwar, *Can. J. Chem.*, 1968, **46**, 507–513.
- 70 G. P. Association, *Physical Properties of Glycerine and Its Solutions*, Glycerine Producers' Association, New York, 1963.
- 71 R. J. Carlton, J. K. Gupta, C. L. Swift and N. L. Abbott, *Langmuir*, 2012, **28**, 31–36.
- 72 I. Stewart, *The static and dynamic continuum theory of liquid crystals*, Taylor and Francis, London, 2004.
- 73 V. V. Belyaev, T. P. Antonyan, L. N. Lisetski, M. F. Grebyonkin, G. G. Slashchova and V. F. Petrov, *Mol. Cryst. Liq. Cryst.*, 1985, **129**, 221–233.
- 74 W. Waclawek, R. Dabrowski and A. Domagala, *Mol. Cryst. Liq. Cryst.*, 1982, **84**, 255–265.
- 75 M. F. Grebyonkin, V. F. Petrov and B. I. Ostrovsky, *Liq. Cryst.*, 1990, **7**, 367–383.
- 76 J. E. Hallett, D. W. Hayward, T. Arnold, P. Bartlett and R. M. Richardson, *Soft Matter*, 2017, **13**, 5535–5542.
- 77 A. V. Egorov, A. P. Lyubartsev and A. Laaksonen, *J. Phys. Chem. B*, 2011, **115**, 14572–14581.
- 78 U. Delabre, C. Richard and A. M. Cazabat, *J. Phys.: Condens. Matter*, 2009, **21**, 464129.
- 79 J. M. Brake, M. K. Daschner, Y.-Y. Luk and N. L. Abbott, *Science*, 2003, **302**, 2094–2097.
- 80 D. S. Miller, X. Wang and N. L. Abbott, *Chem. Mater.*, 2014, **26**, 496–506.